Generation of Land-Clutter Maps for Cognitive Radar Technology

Gaspare Galati and Gabriele Pavan(✉)

Tor Vergata University of Rome, Via Del Politecnico, 1, 00133 Rome, Italy
{Gaspare.Galati,Gabriele.Pavan}@uniroma2.it

Abstract. The concept of cognitive radar is based on an intelligent signal processing obtained by the interaction of the radar with the surrounding environment in order to optimize the radar operation. In the frame of the vast literature on measurement and modelling of the echoes from the environment such as land, vegetation, man-made infrastructures (called *land clutter* or *fixed clutter* in the radar jargon), this paper is aimed to contribute with a practical methodology based on a moveable, lightweight, small and cheap marine radar and its calibration. Live results, related to Radar Cross Section measurements in a typical suburban area, are also shown and analysed. Buildings, streets, highways, car parking areas with different coatings, large and medium size lamp-posts, soil with grass, trees, all in a radius of a very few kilometres, makes this area interesting as far as land clutter characterization is concerned.

Keywords: Land clutter · Radar cross section · Radar calibration
Cognitive radar

1 Introduction

The problem to quantitatively define the operational environment of a radar is one of the main components in cognitive radar applications [1]. For various radar applications, including the surveillance of the airports and of urban and suburban areas for detection of unauthorized vehicles, a clutter map is a very useful detection tool [2, 3]. Detection of targets in land clutter is a challenging problem, as a clutter echo may be orders of magnitude more powerful than the useful echoes due to the targets of interest, making them hardly visible. A careful selection of the radar site may minimize the extent of land clutter, but the related experimental analysis by a set of live measurements with the radar set to be installed may require movements of heavy and bulky equipment.

In this paper, aimed at the widely used X-Band radars, we propose a novel, simpler and practical approach based on the calibration, using standard radar reflectors and processing means, of a cheap and light weight X-band radar, easily movable in the operational site. Live results are presented and discussed.

Section 2 describes the main characteristics of the X-band radar used during the trials and its calibration by means of three standard octahedral corner reflectors. In Sect. 3 we report the experimental results of clutter estimation, showing the basic radar environment characterization by maps of Radar Cross Section. Final considerations and future perspectives are shown in Sect. 4.

Á. Rocha et al. (Eds.): WorldCIST'18 2018, AISC 746, pp. 1463–1470, 2018.
https://doi.org/10.1007/978-3-319-77712-2_141

2 Radar Calibration

The simple and lightweight radar employed for clutter analysis and map generation is a X-band marine radar (model SRT by Simrad/Navico, kindly supplied by their Radar Business Unit in Montagnana, near Florence). It uses a magnetron transmitter with a peak power of 12 kW operating in three different modes for *short*, *medium* and *long* range operations. The pattern of the antenna shows an elevation beam-width of 25° and a horizontal one of 1.35° corresponding to an angular resolution per unit length of about 24 m/km. In reception, the logarithmic amplifier compresses the 95 dB input dynamic range into a video signal from 0 to 2 V. Thanks to the sampling at 50 MHz, followed by 8-bit Analog-to-Digital-Conversion, it is possible to record the matrix (R, θ) (Range, Azimuth) containing all the acquired levels (0–255). The matrix has 2048 rows (or range-bins) and a variable number of columns related to the antenna speed. All trials have been performed with a rotating antenna at 24 Revolutions Per Minute (*RPM*) in the *short range* mode with a pulse length of 50 ns, providing a 7.5 m theoretical range resolution and a band occupancy of 20 MHz. The coefficients of the matrix (R, θ), i.e. the Analog to Digital Converter (ADC) output, or ADC_{level}, represent the received power by the law:

$$P_{rx}[dBm] = \alpha \cdot ADC_{level} - \beta \tag{1}$$

where the constant α [dBm/level] is the step associated to each level, while β [dBm] is related to the noise floor level. The received power is related to the radar parameters of Table 1 by the Radar Equation [4]:

$$P_{rx} = \frac{P_{tx} G_{tx} G_{rx} \lambda^2}{(4\pi)^3 R^4} \cdot \frac{RCS}{L} \tag{2}$$

Table 1. Main Simrad RST radar parameters.

Parameters	Value	Value [dB]
Transmitter type	Magnetron	
Receiver type	Logarithmic, non-coherent	
Transmitted Power: P_{tx}	12 kW	40.8
Antenna Gain: G_{tx},G_{rx}	795	29
Wavelength: λ	3.19 cm	–14.96
Polarization	Horizontal	

For a given distance R, the received power is proportional (in the linear range of the receiver) to the ratio RCS/L, where RCS denotes the Radar Cross Section of the target, while L is the overall result (sum of dBs) of the various losses. The RCS of a target is defined as 4π times the ratio between the power per unit solid angle reflected toward the radar and the power per unit area of a plane wave incident on the target (the latter is

supposed true if the target is far enough from the radar that the incident wave can be considered to be planar rather than spherical). The *RCS* depends on the shape and the characteristic dimensions of the target compared to the radar wavelength. When the wavelength is large enough compared to the target's dimensions, the backscattered electromagnetic field can be described using the optical approximation and the *RCS* is very close to the geometrical one. Using a number N of radar reflectors, with different and known capability to back-scatter the radar signal, it is possible to set N independent measurements of the received power P_{rx} and, via regression techniques, to estimate N parameters of the law P_{rx} vs *RCS* including the losses L. At a first glance it is a linear law, but it may be more complicated than Eq. (1) due to *noise/clutter* level, saturation and other effects. In the linear region, as the line P_{rx} vs *RCS* does not include the (0, 0) point, calibration is possible with $N = 2$, but $N \geq 3$ is preferable to permit quality check by using redundancy.

2.1 Targets: Corner Reflectors and Spheres

Three octahedral Corner Reflectors (CRs), see Fig. 1a, and three metal coated spheres (see Fig. 1b) have been built and used as standard radar reflectors. The size of the three octahedral CRs was chosen in order to cover a 24 dB dynamic range passing from the small CR to the large one. The weight of these CR's (from 0.9 kg to 3.8 kg) is compatible with mounting on a tripod and a simple pole. To reduce the dependence from azimuthal and elevation angles, the CR was mounted in *"catch rain"* position as shown in Fig. 2a. Note that normally, to enhance the radar visibility of vessels, the CR is mounted in the *"up right"* position, i.e. with the axis of symmetry being vertical as shown in Fig. 2b. Figure 2c shows the trihedral of side a (used in the following as an approximation of the octahedral) with a viewing perspective defined by the azimuthal and elevation angles (θ, ψ).

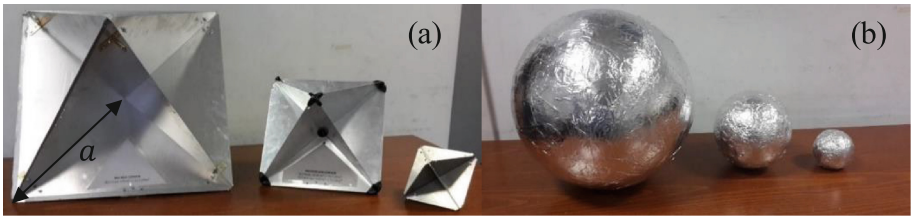

Fig. 1. (a) Three octahedral Corner Reflectors (CRs) with dimension: a=45 cm, a=22.5 cm, a=11.25 cm. (b) Three metal coated spheres with radius: r=20 cm, r=10 cm, r=5 cm.

For the trihedral the theoretical peak of the Radar Cross Section is $4\pi a^4/3\lambda^2$ when $\theta = 45°$ and $\psi = \tan^{-1}\left(1/\sqrt{2}\right) \cong 35.26°$[5]. Starting from *"up right"* position with azimuthal angle $\theta_0 = 45°$, the CR mounted in *"catch rain"* can be obtained rotating (in depression) of an elevation angle $\psi_0 = \tan^{-1}\left(\sqrt{2}\right) \cong 54.74°$. In this way, observing the CR along a horizontal plane passing for the CR centre, the *RCS* can be approximated by the one corresponding to a trihedral observed with an elevation of

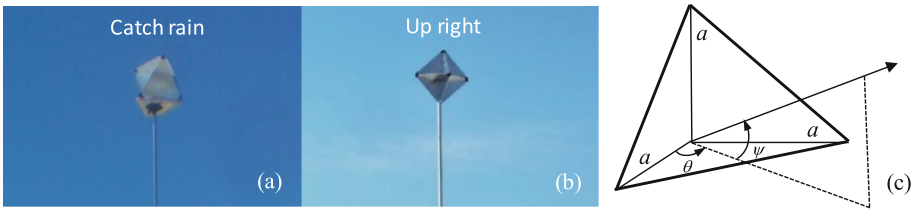

Fig. 2. Octahedral medium corner reflector mounted: (a) in *"catch rain"*. (b) in *"upright"* position. (c) The trihedral approximation.

$\psi_0 = 54.74°$. It results that $RCS(\theta_0, \psi_0) = 2\pi a^4/3\lambda^2$. With λ=3.19 cm, Table 2 shows the *RCS* of CRs, in *"catch rain"* position, using the approximation of a trihedral reflector. In [6] the *RCS* of various types of marine radar reflectors have been measured in an anechoic chamber.

Table 2. X-band *RCS* of CRs in *catch rain* position using the trihedral approximation: $\frac{2\pi a^4}{3\lambda^2}$.

CR type	a [cm]	RCS_{peak} [m^2]	RCS_{peak} [dBm^2]
Small CR	11.25	0.3295	–4.8
Medium CR	22.5	5.27	7.2
Large CR	45.0	84.4	19.3

In order to widen the *RCS* interval for trials, three polystyrene balls (small, medium and large, see Fig. 1b), covered with aluminium foils, have been built. Being λ= 3.19 cm, for the three spheres $2\pi r/\lambda \gg 1$, and the *RCS* is very close to the geometrical cross section, i.e. πr^2. Table 3 shows the *RCS* of the spheres.

Table 3. X-band *RCS* of the three spheres with radius r.

Sphere type	r [cm]	RCS_{peak} [m^2]	RCS_{peak} [dBm^2]
Small	5	0.00785	–21
Medium	10	0.03142	–15
Large	20	0.12566	–9

2.2 Calibration Methods and Losses Estimation

Two different approaches to calibrate the radar are possible. The first technique uses the *ADC* levels and the power levels associated to the mean noise and to the saturation point. In short pulse mode (pulse width 50 ns, B=20 MHz), acquiring samples of only noise, the mean power is: $P_n = Fk_BTB$ = –96 dBm, being the noise figure F=5 dB, T= 290 K (the IEEE reference temperature) and k_B the Boltzmann's constant. From the histogram (based on 21000 noisy samples) of the levels due to noise alone, the mean *ADC* level is 23. Hence, for the law: *ADC* levels vs P_{rx} (dBm) we can define the point

$A \equiv (23, -96)$. Acquiring an entire Plan Position Indicator (PPI) of samples (1687950) due to echoes of noise, near or far buildings, towers, lampposts, … etc., we expected that some near large buildings (less than 300 m from the radar), would put the logarithmic amplifier in saturation. Using the histogram of the levels in an entire PPI, for levels greater than 185 we observe the saturation of the amplifier and we define the level 192 (–5 dB in comparison with the level 185) as the saturation level to whom corresponds the saturation power, defined by the manufacturer as –15 dBm. In conclusion, on the relationship *X*(*Level*)-*P*(*dBm*), a pair of points $A \equiv (23, -96)$ and $B \equiv (192, -15)$ can be used to evaluate the liner law of Eq. (1). It results: $\alpha = 0.4793$ [dBm/level] and $\beta = 107.02$ [dBm]. For level 0 the power tends to –107 dBm, 11 dB below the mean noise.

The second technique of calibration employs three independent measurements obtained (in the same conditions) from the three CRs mounted in the same site (405 m away from the radar). For small, medium and large CRs the mean measured *ADC* levels are 121, 147 and 171 respectively. Being the dimension (side *a*) of medium and large CR two times and four times of the small one, normalizing the CRs *RCS* to the small one, the theoretical *RCS* result 0 dB, 12 dB and 24 dB respectively. Then, on the relationship *X*(*Level*) versus *P*(*dBm*) we can define three points: $A \equiv (121, 0)$, $B \equiv (147, 12)$, $C \equiv (171, 24)$. By linear regression, the slope of the straight line among (*A*, *B*, *C*) results $\alpha = 0.4814$ [dBm/level]. Imposing to the straight line to pass on the mean noise point (23, –96), β results 107.07 [dBm]. The (α, β) values are very close to the ones obtained in the first method.

Once the coefficients (α, β) are defined, the global loss *L* in radar Eq. (2) has been estimated as the value that minimizes the mean square error between the theoretical and the estimated (measured) *RCSs* of the three CRs. For the two methods, Table 4 shows the calibration parameters (α, β) and the estimated losses *L* [dB].

Table 4. Calibration parameters (α, β), estimated loss *L* and standard deviation (*STD*) of the *RCS* estimation for the three CRs.

Calibration method	α [dBm/level]	β [dBm]	*L* [dB]	*STD* [dBm^2]
I method	0.4793	107.02	5.92	0.35
II method	0.4814	107.07	5.61	0.31

As a remark, the relationship between *dBm*'s and *ADC* levels shows a very good linearity in the main interval of interest (i.e. for the clutter echoes – much stronger than noise – which are the main aim if this work), making a precise calibration of the radar feasible, as shown in the ensuing section.

3 Experimental Results

First, we have estimated the noise power and it resulted equal to –95.5 dBm. Second, we have evaluated the level of only clutter in the radar cell under test, i.e. in that cell where the reflector will be positioned for the trials. The cell is 405 m far away from the

radar and its size is 9.6 m × 9 m. For the land clutter (made of small pebbles) it is –77.7 dBm. These values will be compared with the power levels due to CRs and spheres. As shown in the following, noise and clutter levels result to be well below the received power from the CRs.

3.1 RCS Estimation of Corner Reflectors, Spheres, Fixed Target and Land Clutter

Using α=0.4814, β=107.07 and L=5.61 dB, Fig. 3a show the estimated *RCSs* versus the theoretical ones for the three CRs and the three spheres. The estimated *RCSs* show a standard deviation of only 0.31 dBm^2 (see Table 3). The latter has been evaluated considering only the three CRs. For large sphere a light overestimation of the *RCS* (1 dB) is present, while for medium and small spheres more evident overestimations result, mainly for the small sphere (5 dB). Figure 3b shows these overestimations in terms of received power. From Fig. 3b if the radius of the sphere tends to zero, the regression line (dashed line) evaluated from the three measured values tends to –61.7 dBm. But, being the noise and the clutter levels much less than this value, –61.7 dBm can be considered an estimation of the power reflected from the pole on the tripod where the sphere is mounted. The pole is a 2.5 cm diameter metal tube, 3 m height, whose reflectivity is not negligible even in the horizontal polarization.

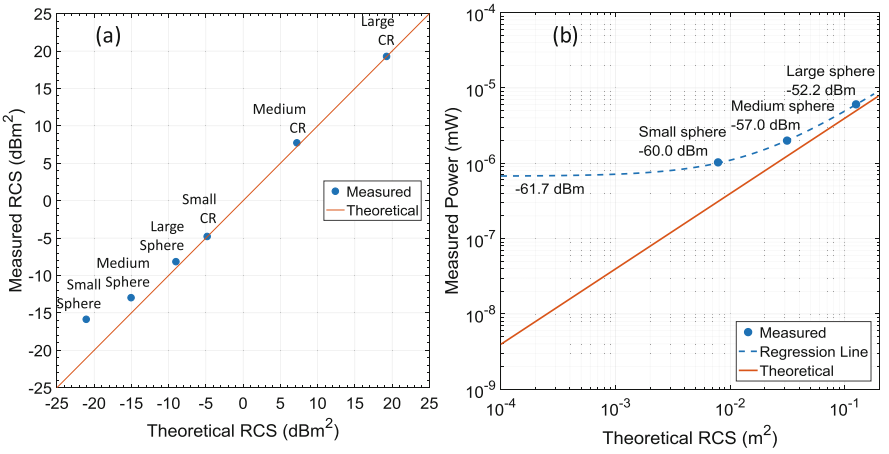

Fig. 3. (a) Estimated (measured) *RCS* (dBm^2) vs Theoretical *RCS* (dBm^2) for all reflectors. (b) Measured Power (mW) vs Theoretical *RCS* (m^2) for small, medium and large spheres.

To evaluate the radar calibration, we have considered three fixed targets, i.e. three identical large lampposts at different distance from radar (see Fig. 4a for two of these lampposts). Figure 4b shows a zoom of a lamppost. The estimated *RCSs* are very similar to each other, as reported in Table 5, and they are of same order as the *RCS* of the large CR. Finally, with low grazing angle (1°), we have estimated the *RCS* for land clutter: $\sigma_{Land}=\sigma^o A$ where σ^o is the *RCS* per *unit area*, while A denotes the area of the

cell. Figure 4c shows the observed surface (grass) at a distance of 1071 m from the radar. The area A of the cell is 9 m $\times$ 25.2 m=227 m^2 and σ^o results 7.25×10^{-4} (i.e. –31.4 dB). At X band σ^o for grass with low grazing angle is about –30 dB [7–9], which is in fairly good agreement with the theory.

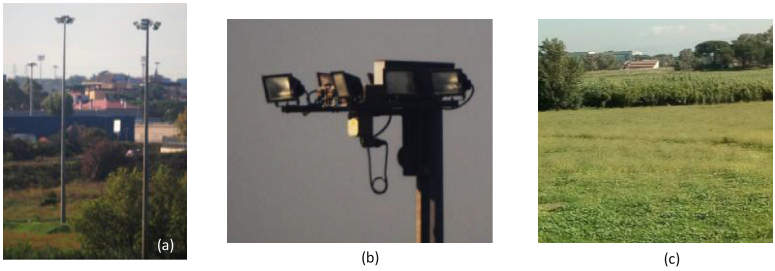

Fig. 4. (a) Large lampposts, 20 m height, at different distances from the radar. (b) Zoom of a lamppost. (c) Cell under test to evaluate the *RCS* per unit area of the land clutter due to grass.

Figure 5 shows an overlay between the *Google Earth* map with the *RCS* map in the suburban environment of Tor Vergata area. Large buildings in the *RCS* map are highlighted, resulting well overlapped with the real ones.

Table 5. *RCS* of three lampposts at different distances from radar.

Radar distance	Lamppost RCS (dBm^2)
360 m	19.7
576 m	18.1
801 m	19.8

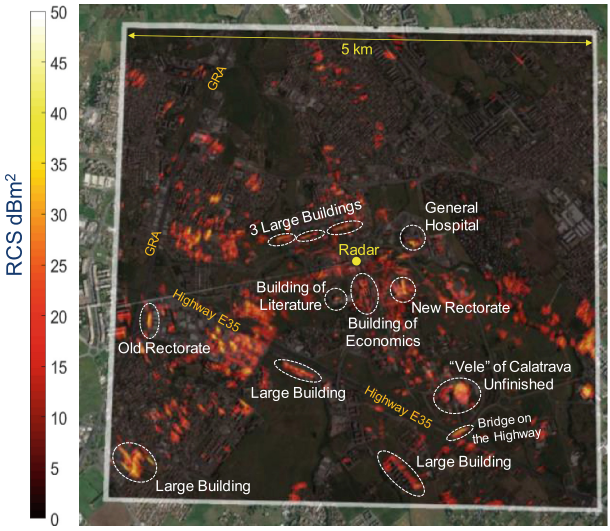

Fig. 5. *RCS* clutter map and *Google Earth* map.

4 Conclusions

Quantitative analysis of disturbing echoes (clutter) in sub-urban and in country areas is possible using a simple, non-coherent marine radar with suited data processing tools. Radar calibration with standard reflectors has been achieved within 1 dB. In such a way, calibrated maps of surface (fixed clutter) are obtained; one application is in the optimal siting of a surveillance radar.

References

1. Guerci, J.R.: Cognitive Radar: The Knowledge-Aided Fully Adaptive Approach. Artech House, Norwood (2010)
2. Nitzberg, R.: Clutter Map CFAR analysis. IEEE Trans. AES **AES-22**(4), 419–421 (1986)
3. Xiangwei, M.: Performance analysis of Nitzberg's clutter map for Weibull distribution. Digit. Sig. Process. **20**(3), 916–922 (2010). https://doi.org/10.1016/j.dsp.2009.10.001
4. Skolnik M.: Introduction to Radar Systems, 3rd edn. McGraw-Hill Education (2002)
5. Doerry, A.W., Brock, B.C.: Radar Cross Section of Triangular Trihedral Reflector with Extended Bottom Plate. SANDIA REPORT SAND2009-2993 (2009)
6. Luke S.: Performance investigation of marine radar reflectors on the market. QINETIQ Report D&TS/SEA/CR0704527/2.0 (2007)
7. Barton, D.K.: Land clutter models for radar design and analysis. Proc. IEEE **73**(2), 198–204 (1985)
8. Nathanson, F.E., Relly, J.P., Cohen, M.N.: Radar Design Principles – Signal Processing and Environment, 2nd edn. Scitech, Medham (1999)
9. Billingsley, J.B.: Low-Angle Radar Land Clutter – Measurements and Empirical Models. William Andrew Publishing, Norwich (2002)